Experimental study of velocity filtered joint density function for large eddy simulation

Danhong Wang and Chenning Tong[a)]
Department of Mechanical Engineering, Clemson University, Clemson, South Carolina 29634-0921

Stephen B. Pope
Sibley School of Mechanical and Aerospace Engineering, Cornell University, Ithaca, New York 14853

(Received 10 May 2004; accepted 25 May 2004; published online 13 August 2004)

The velocity filtered joint density function (VFJDF) used in large eddy simulation and the structure of the subgrid-scale (SGS) velocity are studied experimentally. Measurements are made in the fully developed region of an axisymmetric turbulent jet (with jet Reynolds number $U_jD_j/\nu=40\,000$) using an array consisting of three X-wire probes. Filtering in the cross-stream and streamwise directions is realized by using the array and by invoking Taylor's hypothesis, respectively. On the jet centerline the means of the VFJDF conditional on the SGS turbulent kinetic energy are found to be close to joint normal when the SGS energy is small compared to its mean but has a uniform portion when the SGS energy is large. The latter distribution has not been observed previously and suggests that the SGS velocity contains approximately linear structures and is under local rapid distortion. The results at off-centerline positions are also consistent with the existence of linear structures. Further analyses show that the SGS velocity field with large SGS energy is in nonequilibrium (SGS production exceeds dissipation) and that the degree of nonequilibrium largely determines the shape of the VFJDF. The conditional energy dissipation has moderate dependence on the SGS velocity as expected due to their scale separation. However, the off-diagonal component of the conditional dissipation tensor is non-negligible when the SGS energy is large, at least for the Reynolds number studied. The present study suggests that the different structures and the local rapid distortion observed are important for SGS modeling. The results also suggest that the eddy-viscosity-type models for the SGS stress generally cannot give qualitatively correct predictions for SGS turbulence under local rapid distortion. © *2004 American Institute of Physics*. [DOI: 10.1063/1.1776194]

I. INTRODUCTION

Large-eddy simulation (LES) is gaining increasing importance as an approach for computing turbulent reacting flows.[1–15] In LES of turbulent reacting flows, in addition to the greater difficulties in modeling the subgrid-scale (SGS) scalar fluxes compared to nonreacting flows, the main challenge is to model the effects of the SGS scalar mixing on chemical reactions, because chemical reactions usually occur at scales much smaller than LES filter scales. Therefore to develop improved models for LES of reacting flows, understanding of the mixing of the SGS scalar by the SGS velocity field is essential. As a step toward this goal, we investigate the structure of the SGS velocity field in the present work.

One way to account for the effects of the SGS mixing in LES is to model the scalar filtered density function (FDF), which is essentially the weighted distribution of the scalar in a grid cell and which can be used to obtain the filtered reaction rate. The scalar FDF method solves a FDF transport equation in which the effects of reactions on the evolution of the FDF are in closed form while the SGS transport and mixing terms are modeled. The capabilities of the FDF method have recently been demonstrated.[10] However, in this approach the resolvable-scale velocity field is obtained through other means (e.g., conventional LES in which the filtered Navier–Stokes equations are solved). The SGS scalar transport term is in effect modeled through a SGS scalar eddy diffusivity obtained in the velocity LES. Furthermore, the SGS scalar mixing is modeled independent of the velocity field. A more advanced approach solves the velocity-scalar filtered joint density function (FJDF) transport equation, which is developed from the velocity-scalar joint probability density function (JPDF) method.[16] In this approach scalar transport by the SGS velocity is also in closed form. In addition, because molecular mixing is local in both composition and velocity spaces, inclusion of velocity information into mixing models can potentially lead to a more realistic description of the SGS mixing. This approach has recently been established successfully.[15] To develop improved models used in the velocity-scalar FJDF approach, understanding of the physics of the SGS velocity and scalar fields is essential. Scalar FDF and its transport equation have been previously investigated.[17,18] In the present work we study the velocity FJDF (VFJDF) and its transport equation to elucidate the fundamental SGS physics of the velocity field, which will provide a basis for studying the velocity-scalar FJDF. Improved understanding of the SGS physics

[a)]Author to whom correspondence should be addressed. Electronic mail: ctong@ces.clemson.edu

will also be important for modeling the SGS stress in LES of nonreacting flows.

The VFJDF is defined as[2,10]

$$f_u(\mathbf{v};\mathbf{x},t) = \int \prod_{i=1}^{3} \delta[u_i(\mathbf{x}',t) - v_i] G(\mathbf{x}' - \mathbf{x}) d\mathbf{x}' = \left\langle \prod_{i=1}^{3} \delta[u_i - v_i] \right\rangle_L, \quad (1)$$

where $\mathbf{v}$, δ, and G are the sample-space variable for the fluid velocity $\mathbf{u}$, the Dirac delta function, and the filter function, respectively. The integration is over all physical space. A filtered variable is denoted as $\langle\cdot\rangle_L$. The symbol $\langle\cdot\rangle$ is used for ensemble averages. Thus the VFJDF is the filtered fine-grain density, $\langle\Pi_{i=1}^{3}\delta[u_i - v_i]\rangle_L$, and represents the weighted joint distribution of the velocity components in a grid cell. For a top-hat (box) filter $f_u(\mathbf{v})d\mathbf{v}$ is the fraction of fluid in the grid cell whose velocity components are between v_i and $v_i + dv_i$. A VFJDF obtained using a non-negative filter satisfies all the properties of a JPDF.

The transport equation of the VFJDF can be obtained using its definition [Eq. (1)] and the Navier–Stokes equations:[13,16]

$$\frac{\partial f_u}{\partial t} + v_j \frac{\partial f_u}{\partial x_j} = \frac{\partial \langle p\rangle_L}{\partial x_i}\frac{\partial f_u}{\partial v_i} + \frac{\partial}{\partial v_i}\left\{\left\langle \frac{\partial p''}{\partial x_i}\middle|\mathbf{u}=\mathbf{v}\right\rangle_L f_u\right\} - \frac{\partial}{\partial v_i}\left\{\left\langle \nu\frac{\partial^2 u_i}{\partial x_j \partial x_j}\middle|\mathbf{u}=\mathbf{v}\right\rangle_L f_u\right\}, \quad (2)$$

where $\langle\cdot|\mathbf{u}=\mathbf{v}\rangle_L$ denotes a conditionally filtered variable conditional on the velocity vector and double prime denotes SGS variables. The left-hand side is the time rate of change of the VFJDF and transport of VFJDF in physical space. The terms on the right-hand side (RHS) represent transport in velocity space by the resolvable-scale pressure gradient, by the SGS pressure gradient, and by viscous acceleration. Galilean invariance of Eq. (2) has been shown.[19] The SGS pressure gradient and viscous terms can also be written as

$$\frac{\partial}{\partial v_i}\left\{\left\langle \frac{\partial p''}{\partial x_i}\middle|\mathbf{u}=\mathbf{v}\right\rangle_L f_u\right\} - \frac{\partial}{\partial v_i}\left\{\left\langle \nu\frac{\partial^2 u_i}{\partial x_j \partial x_j}\middle|\mathbf{u}=\mathbf{v}\right\rangle_L f_u\right\} = \frac{\partial^2}{\partial v_i \partial x_i}\{\langle p''|\mathbf{u}=\mathbf{v}\rangle_L f_u\} + \frac{\partial^2}{\partial v_i \partial v_k}\{\langle p'' s_{ik}|\mathbf{u}=\mathbf{v}\rangle_L f_u\} + \nu\frac{\partial^2 f_u}{\partial x_j \partial x_j} - \frac{\partial^2}{\partial v_i \partial v_k}\{\langle \epsilon_{ik}|\mathbf{u}=\mathbf{v}\rangle_L f_u\}, \quad (3)$$

where s_{ik} and $\epsilon_{ik} = \nu(\partial u_i/\partial x_j)(\partial u_k/\partial x_j)$ are the strain rate and the dissipation tensor, respectively. The terms on the RHS of Eq. (3) are mixed transport of VFJDF by the SGS pressure in physical and velocity spaces, transport in velocity space by the-pressure-rate-of-strain, viscous diffusion in physical space, and transport in velocity space by the velocity dissipation tensor. Gicquel *et al.*[13] have developed a stochastic model based on the generalized Langevin model developed for the probability density function (PDF) method.[20] Comparisons between results using the VFJDF approach show improvements over those using conventional LES with Smagorinsky and dynamic Smagorinsky models in several aspects such as SGS stress and SGS energy production, and are comparable in other aspects.

In the present work we study the characteristics of the VFJDF and some of the SGS terms in the VFJDF equation. Unlike PDFs, a VFJDF is not a statistic, but a random process, and must be characterized statistically. For a filter size smaller than the integral length scale, the mean VFJDF approximately equals the velocity JPDF, which is generally not far from joint Gaussian in regions of fully developed flows without large-scale intermittency.[21,22] Issues in modeling the JPDF equation have also been studied in terms of Lagrangian statistics for stochastic modeling[23] which can be used to model the Lagrangian PDF equation.

Other important characteristics of the VFJDF can be revealed by its conditional means. Previous investigations of conditional scalar FDF (SGS PDF) and scalar-scalar-dissipation FJDF have provided important characteristics of the SGS scalar field. The SGS scalar has been found to be in quasi-equilibrium (SGS production equal to or smaller than dissipation) and nonequilibrium (SGS production exceeds dissipation) for small and large SGS scalar variance, respectively.[17,18] Here for convenience we refer both the cases of SGS production equal to and smaller than dissipation as quasi-equilibrium because the SGS scalar has very similar characteristics for the two cases. The FDF and the terms in its transport equation in these two regimes have qualitatively different characteristics. For quasi-equilibrium SGS scalar the FDF is on average close to Gaussian and the scalar dissipation has only moderate dependence on the SGS scalar. These properties are similar to those of unfiltered scalar fluctuations in fully developed turbulent flows. However, for nonequilibrium SGS scalar at large SGS scalar variance, the FDF is bimodal and the scalar dissipation depends strongly on the SGS scalar. The SGS scalar is also characterized by the existence of diffusion-layer-like structure (ramp cliffs). These characteristics are similar to the scalar PDF in the early stages of initially binary mixing.[24] Therefore, when used as a conditioning variable for the conditional scalar FDF, the SGS scalar variance can reveal the structure of the SGS scalar that is otherwise averaged out, providing important new SGS physics. This is partly because the SGS variance is an important variable in the inertial-range dynamics and for characterizing the state of SGS mixing. Since the conditional scalar FDF for different SGS variance are dominated by different structures and dynamics, they can potentially be modeled more accurately than the unconditioned FDF (or PDF), leading to improved LES statistics. Therefore, such conditional FDFs are important for studying the SGS scalar and modeling SGS mixing.

The results for the SGS scalar suggest that the equilibrium and nonequilibrium regimes and different structures may also exist in the SGS velocity field. An important variable analogous to the SGS scalar variance is the SGS kinetic energy, $k_L = \frac{1}{2}\langle u_i'' u_i''\rangle_L$, which can potentially be used to reveal new structures of the SGS velocity. Thus we investigate the VFJDF and the SGS terms in the FJDF transport equation by analyzing their conditional means with the SGS kinetic energy as a conditioning variable. Another variable that may be

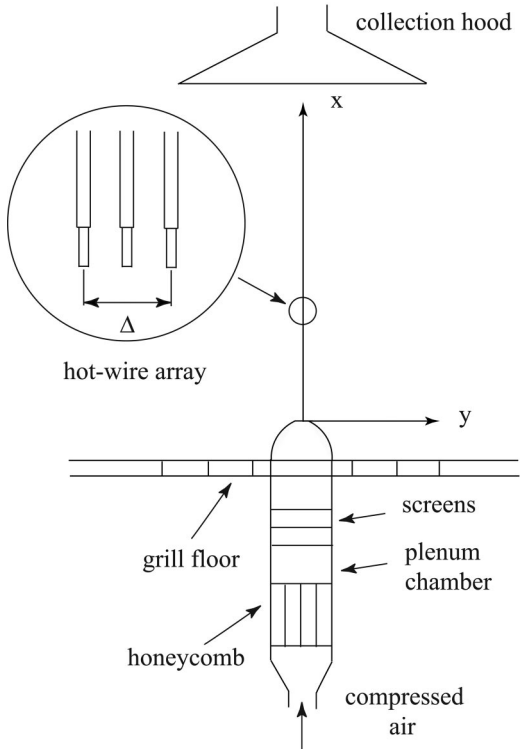

FIG. 1. A schematic of the experimental setup including a magnified view of the hot-wire array.

important in characterizing the SGS velocity is the SGS dissipation time scale (the ratio of the SGS energy to the filtered energy dissipation $\epsilon_L \equiv \langle \epsilon \rangle_L$), which we will also use as a conditioning variable. These variables are important for characterizing the SGS dynamics and therefore can potentially bring out important structures of the SGS velocity, leading to improved LES statistics. The scaling properties of k_L and ϵ_L have been studied previously.[25,26] They have also been used as conditioning variables to investigate the conditional PDFs of velocity increments,[26] which have provided important understanding of the structure of the SGS velocity.

In the present study we use experimental data obtained in the fully developed region of an axisymmetric turbulent jet to analyze the unclosed terms in the VFJDF and its transport equation. The following sections are organized as follows. In Sec. II we outline the experimental apparatus and flow conditions. The experimental results are discussed in Sec. III, followed by the conclusions (Sec. IV).

II. FLOW FACILITIES AND APPARATUS

The jet facility was housed in a large, air-conditioned room. The jet assembly was mounted vertically on a 5×5 ft^2 grill portion of the floor to allow the flow of entrainment air (Fig. 1). The flow downstream of the nozzle was surrounded by a circular screen (1/16 in. mesh size) of 6 ft in diameter to reduce the disturbances in the room. A collection hood was installed at a downstream distance of 260 nozzle diameters (3.9 m) to minimize the effects of the ceiling on the jet. The hood was connected to an exhaust fan with the flow rate adjusted by a throttle. The jet nozzle had a fifth-order polynomial profile with a large contraction ratio ($\approx$100), producing a nearly top-hat velocity profile at the nozzle exit.

All measurements were made for a jet exit velocity U_j of 40 m/s. The jet Reynolds number Re_j based on the nozzle diameter D_j and the jet exit velocity $(U_j D_j/\nu)$ was 40 000 where ν is the kinematic viscosity. The corresponding Taylor microscale Reynolds number $R_\lambda = \langle u_1^2 \rangle^{1/2} \lambda / \nu$ was $\approx$230, where $\langle u_1^2 \rangle^{1/2}$ is the rms streamwise velocity fluctuation and λ is the Taylor microscale. Refer to Table I for other flow parameters. Data were collected at a downstream distance of $x/D_j = 80$, well into the self-similar (fully developed) region of the jet. We limit our off-centerline measurement location to $y/x = 0.1$ to avoid flow reversal and to minimize errors associated with employing Taylor's hypothesis, where y is the radial distance from the jet centerline. The mean axial velocity on the jet centerline U_c at this downstream location was 3.07 m/s and the resulting U_j/U_c value was comparable to previous results.[27–29] The Kolmogorov scale $\eta = (\nu^3/\epsilon)^{1/4}$ was 0.16 mm, where $\langle \epsilon \rangle$ is the mean turbulent kinetic energy dissipation rate. Under these flow conditions the Kolmogorov frequency of the signals $(U_c/(2\pi\eta) = 2.5$ kHz) was fully resolved by the sensors.

Measurements of the VFJDF and the conditionally filtered variables require spatial filtering of turbulent velocity fields. Due to the difficulties in obtaining three-dimensional data experimentally, two-dimensional (streamwise and radial directions) filtering was employed in the present study. The streamwise filtering was performed by invoking Taylor's hypothesis and the cross-stream filtering was realized with three hot-wire sensors aligned in the cross-stream direction. To minimize the error associated with invoking Taylor's hypothesis, instantaneous convection velocity obtained by low-pass filtering the streamwise velocity component was used. The filter size for this purpose is twice the largest averaging domain size for obtaining filtered variables so that the convection velocity is relatively uniform within an averaging domain.

The array filter technique was proposed and studied by Tong *et al.*[30] for measurements in the atmospheric boundary layer and has been used by a number of authors to study the SGS stress[30–34] and conditional FDF.[17] Two-dimensional filtering has been demonstrated to provide a very good approximation of three-dimensional filtering, with errors of $\approx$5% for the rms of the resolvable-scale variables.[30] Previous studies of scalar FDF used box filters[17,18,35] because a

TABLE I. Flow parameters on the jet centerline at $x/D_j = 80$.

$\langle U \rangle$	$\langle u_1^2 \rangle^{1/2} (\langle u_1^2 \rangle)$	$\langle u_2^2 \rangle^{1/2} (\langle u_2^2 \rangle)$	R_λ	$\langle \epsilon \rangle$	η	ℓ
3.07 m/s	0.73 m/s (0.533 m^2/s^2)	0.61 m/s (0.372 m^2/s^2)	233	5.22 m^2/s^2	0.16 mm	75 mm

scalar FDF obtained with a box filter is easily interpreted. In this study we also use box filters to maintain consistency between the velocity and scalar fields. Our streamwise filter is, to a very good approximation, a box filter with a transfer function $\hat{G}_1(\kappa_1)=\sin(\kappa_1\Delta/2)/(\kappa_1\Delta/2)$. The cross-stream array filter has a transfer function $\hat{G}_2(\kappa_2)=\frac{1}{3}+\frac{2}{3}\cos(\kappa_2\Delta/2)$ which is somewhat narrower than a true box filter in the wavenumber space. Therefore, the array filter tends to overestimate the SGS variance. Our estimates using the spectral model for inertial-range isotropic turbulence show that the array filter overestimates the mean SGS energy by 13%. The mean SGS variances $\langle u_1''^2\rangle$ and $\langle u_2''^2\rangle$ are overestimated by 16% and 10%, respectively. This difference is because the Φ_{11} component of the isotropic spectral tensor, $\Phi_{ij}=(1/4\pi)\alpha\epsilon^{2/3}\kappa^{-11/3}(\delta_{ij}-\kappa_i\kappa_j/\kappa^2)$, comes mostly from the κ_2 (and κ_3) direction; therefore the cross-stream filter has a greater impact on $\langle u_1''^2\rangle$ than on $\langle u_2''^2\rangle$. Here α is the Kolmogorov constant.

These errors in estimating the SGS variances are not negligible but are not expected to have significant effects on the measured VFJDF since a much larger change in k_L is needed to alter the shape of the conditional VFJDF (see Sec. III). It is not clear how to predict the direct impact of the differences between the array filter and the box filter transfer functions on the VFJDF. However, our previous studies[17,18,35] of scalar FDF and scalar-scalar-dissipation FJDF showed that even a one-dimensional filter produced the same shapes for the FDFs as a two-dimensional box-array filter. Only the quantitative dependences (e.g., the dependence of the conditional kurtosis on the SGS scalar variance) are altered. These results suggest that the shapes of the FDFs are not affected by the details of the filter employed. We also tested a one-dimensional box filter for VFJDF and the same qualitative results are obtained as the two-dimensional box-array filter. Therefore, we expect that the box-array filter will produce VFJDF statistics similar to those using a true two-dimensional box filter.

In the present study three filter widths 10, 20, and 40 mm were used. These correspond to $\Delta/\ell=0.13$, 0.27, 0.53 and $\Delta/\eta=63$, 125, 250, respectively, with the largest being close to the integral length scale ℓ. Here $\ell=75$ mm is estimated using $\langle u_1^2\rangle^{3/2}/\langle\epsilon\rangle$. This value is close to a value of 80 mm estimated using the empirical formula given by Tennekes and Lumley.[36] The percentages of kinetic energy contained in the SGS scales are 21.0%, 34.0%, and 52.7% for the three filter sizes, respectively.

Velocity measurements were made with three X-wire probes operated by TSI IFA 100 hot-wire anemometers with an overheat ratio of 1.8. The probes were calibrated using a modification of a method by Browne *et al.*[37] In this method a velocity-voltage relation at zero yaw angle for each wire was obtained. A yaw-angle-effective-wire-angle relation was determined with yaw-angle calibrations at a fixed velocity (3 m/s in the present study). The effective angles were then used as "geometric" wire angles in computing the two velocity components. The outputs from the hot-wire anemometers were low-pass filtered at 5 kHz and amplified by Krohn-Hite 3364 filters. The signals were digitized at 10 k samples/second by a 12-bit National Instrument A/D converter (PCI-6071E) which has a maximum sampling rate of 1.25×10^6 samples/second so that the interchannel delay is much shorter than the sample interval.

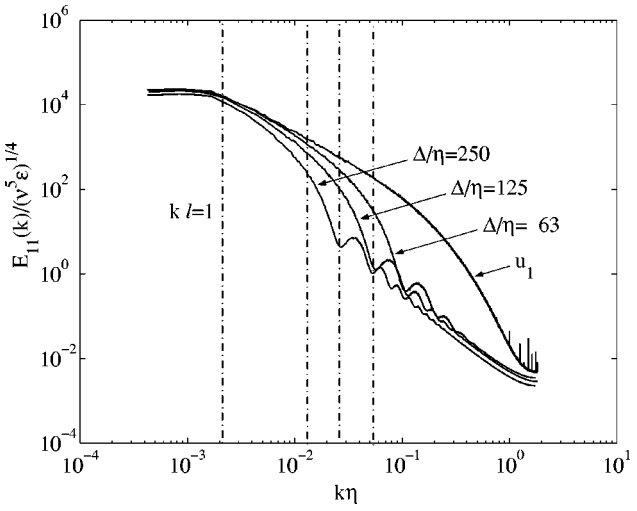

FIG. 2. Spectra of the streamwise velocity and resolvable-scale velocity. The wave number and the spectra are normalized by Kolmogorov length and velocity scales. The filter wave number $\kappa_\Delta=\pi/\Delta$ for each filter width is marked by a dashed vertical line. The lobes at higher wave numbers are due to the inherent leakage in spectral space of box filters. The left most dashed vertical line marks the integral-scale wave number.

In the present study most of the statistics computed are conditional statistics with two to four conditioning variables. To obtain these conditional statistics at a reasonable level of convergence, a large amount of data is needed. The precise number of samples to achieve a given confidence level, however, is difficult to estimate because of the complex statistical characteristics of the conditional samples and the interdependence among the conditioning variables. Therefore we use an empirical approach in which the convergence is monitored when the sample size is increased until good convergence is achieved. We find that 6×10^7 data samples are sufficient.

III. RESULTS AND DISCUSSIONS

In this section the results of the measured conditional VFJDF and some of the terms in the VFJDF transport equation are presented. The filter sizes (Δ) used for obtaining resolvable- and subgrid-scale variables are 63η, 125η, and 250η, or 0.13ℓ, 0.27ℓ, and 0.53ℓ, respectively. The spectra of the full and the resolvable-scale streamwise velocities normalized by Kolmogorov length and velocity scales are given in Fig. 2.

We first briefly discuss the SGS kinetic energy which is the primary conditioning variable in our analyses of VFJDF. The PDF of the SGS kinetic energy is close to log normal,[26,38] indicating that it is intermittent and has the characteristics of an inertial-range variable. However, the sizes of the two-dimensional filter used in this study range from approximately one-half to one-eighth of the integral length scale, therefore there is significant anisotropy in the subgrid scales. The cross-stream filter introduces additional anisotropy since it overestimates $\langle u_1''^2\rangle$ more than $\langle u_2''^2\rangle$ (the result-

TABLE II. SGS variances on the jet centerline at $x/D_j=80$.

$\Delta/\eta(\Delta/\ell)$	$\langle u_1''^2\rangle(\mathrm{m}^2/\mathrm{s}^2)$	$\langle u_2''^2\rangle(\mathrm{m}^2/\mathrm{s}^2)$	$\langle u_1''^2\rangle/\langle u_2''^2\rangle$	$\langle\langle u_1''^2\rangle_L\|k_L\rangle/\langle\langle u_2''^2\rangle_L\|k_L\rangle$
63 (0.13)	0.105	0.087	1.20	1.21 ($k_L/\langle k_L\rangle=1.06$), 1.30 ($k_L/\langle k_L\rangle=4.7$)
125 (0.27)	0.174	0.133	1.31	1.26 ($k_L/\langle k_L\rangle=1.00$), 1.49 ($k_L/\langle k_L\rangle=3.8$)
250 (0.53)	0.238	0.203	1.35	1.31 ($k_L/\langle k_L\rangle=0.97$), 1.56 ($k_L/\langle k_L\rangle=3.0$)

ing $\langle u_1''^2\rangle/\langle u_2''^2\rangle$ is 1.31 for $\Delta/\eta=125$). Due to the anisotropy in the measured SGS variances, using $k_L=\frac{1}{2}(\langle u_1''^2\rangle_L+\langle u_2''^2\rangle_L)$ to sample the velocity field will cause a bias toward the conditional SGS fields with large $\langle u_1''^2\rangle_L$, resulting in even larger conditional anisotropy. Therefore, the conditional SGS fields may not reflect the true average structure of the SGS velocity field. If both $\langle u_1''^2\rangle_L$ and $\langle u_2''^2\rangle_L$ are used as conditioning variables, conditional SGS fields with different levels of anisotropy can be obtained. However, adding a conditioning variable requires a substantial increase in the already large data size. Therefore, we use a modified conditioning variable $\frac{1}{2}(\langle u_1''^2\rangle_L+a\langle u_2''^2\rangle_L)$ to obtain conditional VFJDFs. For convenience we still use the symbol k_L for this variable in the rest of the paper (but the true SGS energy is used to normalize the VFJDF and other variables). In this variable the u_2 component has a larger weight ($a=1.7$) and the resulting conditional SGS velocity fields for both small and larger SGS energy have conditional SGS variance ratios (anisotropy) similar to the unconditioned SGS fields (Table II).

A. The conditional VFJDF

The mean VFJDF conditional on the SGS energy and the resolvable-scale velocity $\langle f_u|k_L,\langle\mathbf{u}\rangle_L\rangle$ measured on the jet centerline with a filter size of 125η is shown in Figs. 3(a) and 3(b). Note that for a specified resolvable-scale velocity, the SGS velocity is equivalent to the total velocity. For convenience we use u_i'' and omit the sample-space variables v_i when plotting the VFJDF and other statistics. The VFJDF is normalized by $(2k_L)^{1/2}$. For small SGS energy ($k_L/\langle k_L\rangle<1$) the conditional FJDF has a similar shape to the velocity JPDF [Fig. 3(e)] which appears to be close to joint Gaussian [also see Figs. 4(a) and 4(d)]. The SGS velocity components are essentially uncorrelated on the jet centerline.

For large SGS energy (generally $k_L/\langle k_L\rangle>3$) the VFJDF [Fig. 3(b)] has an approximately uniform region near the center ($|\mathbf{v}|/\langle 2k_L\rangle^{1/2}\leqslant 1.0$). Beyond this region the VFJDF decreases rapidly (appears to be faster than joint-Gaussian). The VFJDFs for the other filter scales shown in Figs. 3(c) and 3(d) have similar shapes as $\Delta/\eta=125$, although for $\Delta/\eta=63$ the VFJDF has a somewhat steeper edge around the uniform region. The form of the VFJDF depends only weakly on $\langle u_i\rangle_L$; negative streamwise fluctuations tend to clip the negative side of the VFJDF and vice versa (not shown).

To examine the VFJDF in a more quantitative manner we also compute the FDF of the velocity magnitude $q\equiv(u_1''^2+u_2''^2)^{1/2}$. For a VFJDF with a uniform region of radius q_0, the FDF of q, P_q, is linear for $q\leqslant q_0$ and is zero beyond q_0 [$q_0=2^{1/2}$ if q is normalized by $(2k_L)^{1/2}$]. Figure 4 shows the conditional FDF of q for the three filter scales. For small $k_L/\langle k_L\rangle$ the FDF on the jet centerline is close to that obtained from a two-dimensional joint Gaussian distribution whereas for large $k_L/\langle k_L\rangle$ it deviates from the Gaussian predictions, regardless of the filter scales. For the latter cases the FDF has an approximately linear portion up to $q=0.5$, indicating an approximately uniform portion of the VFJDF within $q<0.5$. The approximately linear portion for the Gaussian prediction is much smaller (in fact any JPDF that has zero derivatives at the origin will result in a linear portion). In addition, the peak of the FDF is at a larger q value compared to the Gaussian case, and beyond it the FDF decreases much faster, further indicating that the VFJDF is more compact than the Gaussian JPDF and is closer to a uniform distribution. Here the PDF of q corresponding to a two-dimensional joint Gaussian distribution, $N(\langle u_1''^2\rangle_L^{1/2},\langle u_2''^2\rangle_L^{1/2})$ with standard deviations $\langle u_1''^2\rangle_L^{1/2}$ and $\langle u_2''^2\rangle_L^{1/2}$, is obtained by integrating N along a circle of radius q. The means in the joint Gaussian distribution are zero by the definition of the SGS velocity and correlation between u_1'' and u_2'' is close to zero on the jet centerline. In Fig. 4(d) we also plotted the PDF of the magnitude of the total (unfiltered) velocity vector. It follows the Gaussian prediction closely. Therefore, the VFJDF for small SGS energy has a similar shape to the velocity JPDF measured at the same location which is in the fully developed region of the turbulent jet.[22] The quantitative difference is due to the different ratios of the streamwise to the cross-stream velocity variances. Because a fully developed jet is in quasi-equilibrium, the similarity between the VFJDF and the JPDF suggests that the SGS velocity is also in quasi-equilibrium when the SGS energy is small.

Uniform joint distributions have not been previously observed in a fully developed turbulent jet. The qualitatively different VFJDF shapes for small and large SGS energy suggest that the SGS velocity has different structures under these conditions. A possibility for the SGS velocity to have a uniform VFJDF is that it contains structures in which the velocity has an approximately linear trend in physical space. One such structure is (local) plane strain fields, which we examine in the following.

When a plane strain field is sampled by a two-dimensional filter, a two-dimensional cut of such a structure is obtained. The orientation of the cut relative to the structure is generally random because the structure may be convected through the probes with a random orientation. We first discuss the case in which the normal vector of the two-dimensional cut (the filter plane) is fixed with respect to the structure and then examine the effects of random orientation. A plane strain field with a random orientation is shown in Fig. 5(a). Figure 5(b) gives an example of the conditional

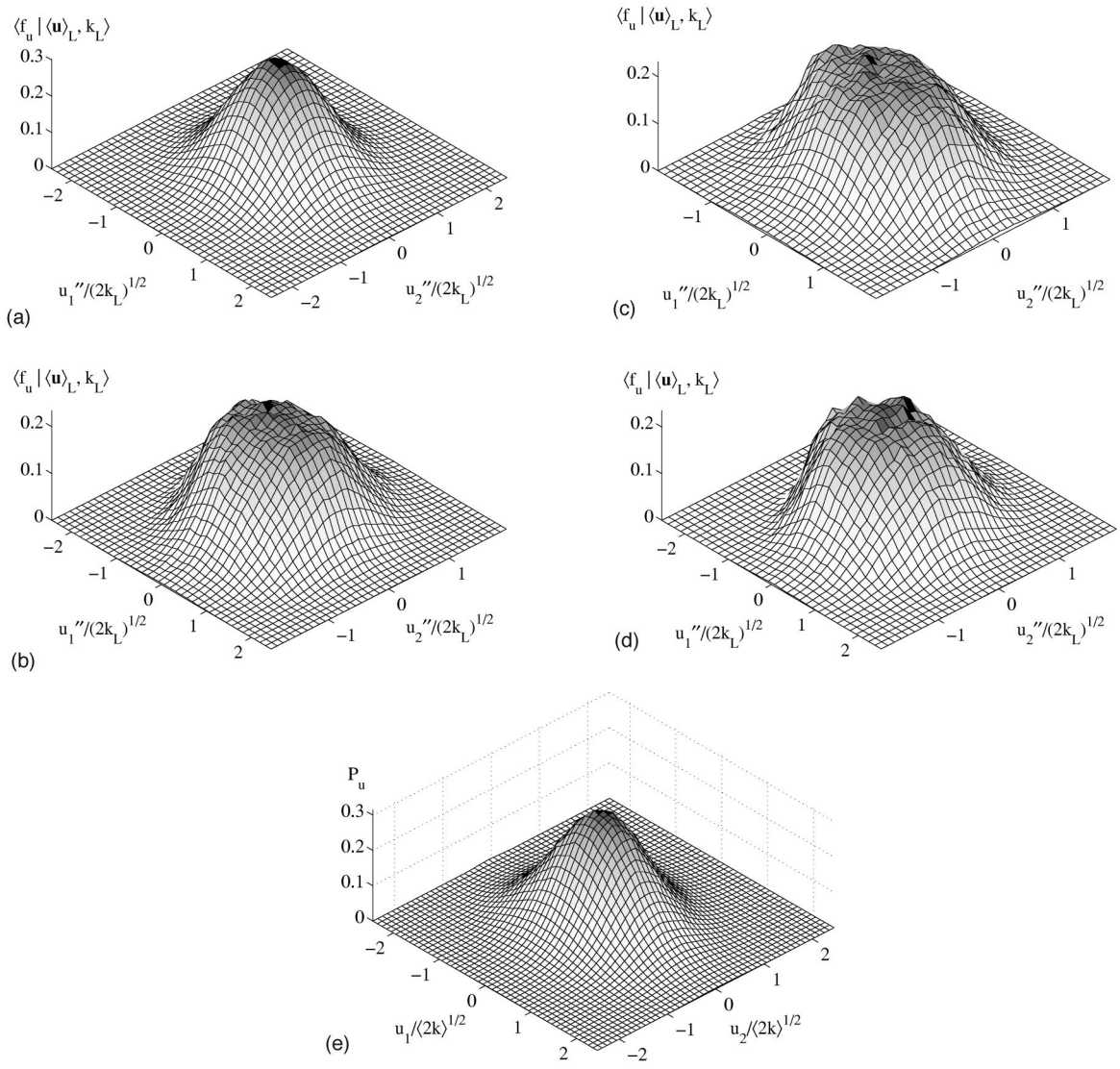

FIG. 3. Conditional mean of the VFJDF on the jet centerline for $\langle u_1\rangle_L=\langle u_1\rangle$ and $\langle u_2\rangle_L=0$ (a–d). (a) $k_L/\langle k_L\rangle=1.2$, $\Delta/\eta=125$; (b) $k_L/\langle k_L\rangle=4.6$, $\Delta/\eta=125$; (c) $k_L/\langle k_L\rangle=5.9$, $\Delta/\eta=63$; (d) $k_L/\langle k_L\rangle=3.0$, $\Delta/\eta=250$. The VFJDF has a uniform portion for large k_L values. (e) The joint PDF of the fluctuating velocity components u_1 and u_2. The VFJDF for $k_L/\langle k_L\rangle<1$ has a similar shape as the JPDF.

velocity field, which is qualitatively consistent with a plane strain field. Here the streamlines are computed based on the velocity vectors from the three X wires. Although the array data are only partially resolved in the cross-stream direction, they contain most of the SGS information near the filter scale and some information at scales much smaller than the filter scale because the data are fully resolved in the streamwise (time) direction. (The accuracy of the array technique is discussed in Sec. II and elsewhere.[30,31]) Therefore, the flow field in Fig. 5(b) is a sufficiently accurate representation of a conditional SGS velocity field. As shown in Fig. 5(a) the velocity components in the filter plane in a coordinate system that is fixed to the flow structure can be represented as $u_1'=a\xi_1$, $u_2'=-b\xi_2$ ($a>0$ and $b>0$). If the filter plane coincides with the plane of strain then a and b are equal. The streamwise velocity component u_1 and the cross-stream component u_2 defined in the laboratory measurement coordinate system [with the streamwise unit vector $\mathbf{x}/|\mathbf{x}|=(x_{\xi_1},x_{\xi_2})$ in the ξ_1-ξ_2 coordinate system] then are $a\xi_1x_{\xi_1}-b\xi_2x_{\xi_2}$ and $-(a\xi_1x_{\xi_2}+b\xi_2x_{\xi_1})$, respectively. The JPDF of u_1 and u_2 can be expressed as the JPDF for the probe to sample (ξ_1,ξ_2):

$$P_{u_1u_2}(v_1,v_2)=P_{\xi_1\xi_2}(\hat{\xi}_1,\hat{\xi}_2)\left|\frac{\partial(v_1,v_2)}{\partial(\hat{\xi}_1,\hat{\xi}_2)}\right|^{-1}$$
$$=P_{\xi_1\xi_2}(\hat{\xi}_1,\hat{\xi}_2)/|ab|, \tag{4}$$

where $|\partial(v_1,v_2)/\partial(\hat{\xi}_1,\hat{\xi}_2)|$ is the Jacobian, and a hat denotes a sample-space variable. Because the samples have equal weight in a grid cell, $P_{\xi_1\xi_2}(\hat{\xi}_1,\hat{\xi}_2)$ and therefore $P_{u_1u_2}(v_1,v_2)$ are uniform. Equation (4) also shows that the uniform part of VFJDF is independent of the orientation of the probe relative to the flow structure.

The extent of the uniform distribution in the v_1-v_2 plane (the velocity space) is determined by the velocity at the boundary of the grid cell. For a square box filter ($a=b$), the

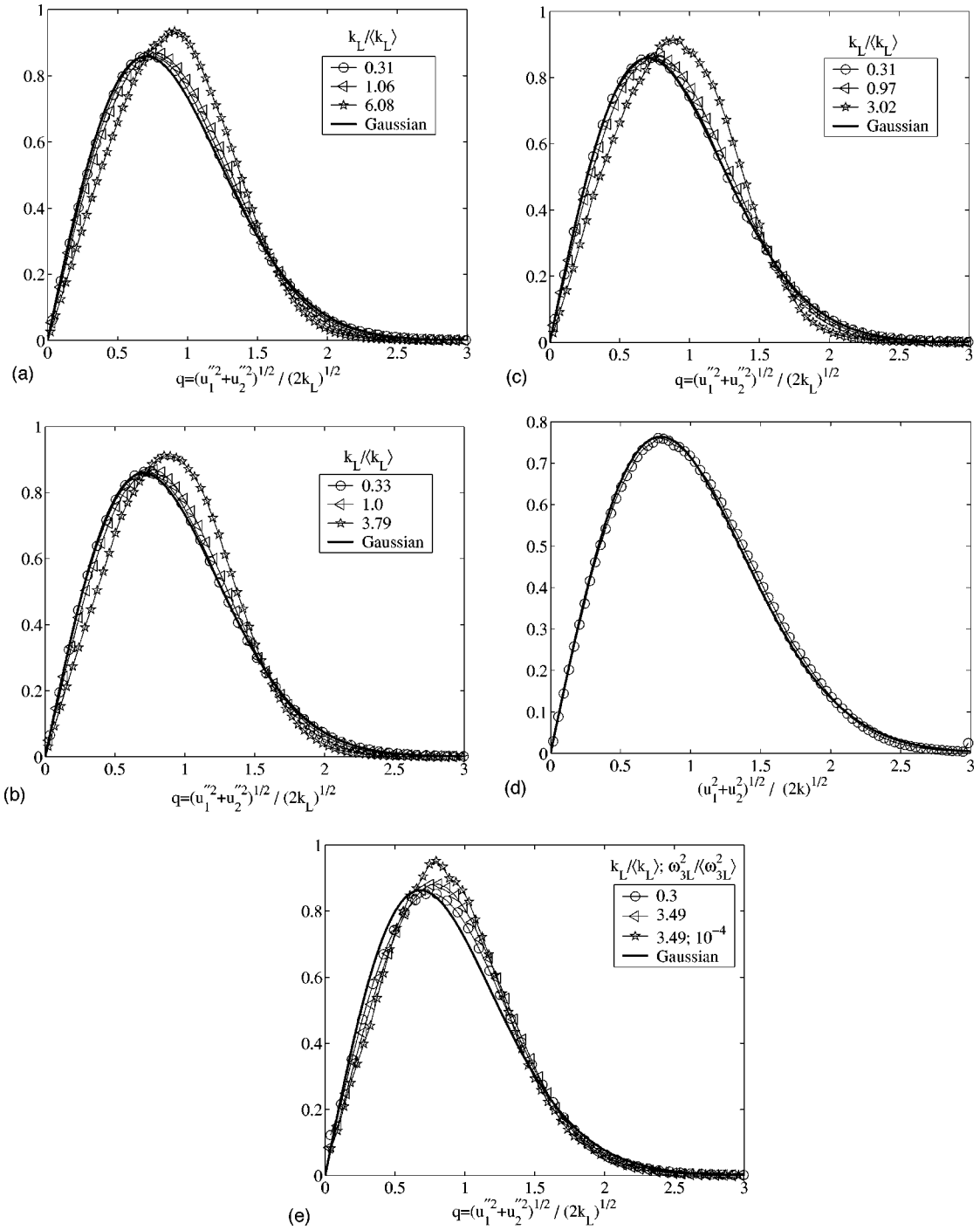

FIG. 4. Conditional mean of the FDF of $q=(u_1''^2+u_2''^2)^{1/2}$ on the jet centerline for $\langle u_1\rangle_L=\langle u_1\rangle$ and $\langle u_2\rangle_L=0$ (a–c): (a) $\Delta/\eta=63$; (b) $\Delta/\eta=125$; (c) $\Delta/\eta=250$. For $k_L/\langle k_L\rangle<1$ the FDF is also close to the Gaussian prediction. For $k_L/\langle k_L\rangle>1$ the FDF is approximately linear for $q<0.5$, consistent with a uniform VFJDF. (d) The PDF of $(u_1^2+u_2^2)^{1/2}$ on the jet centerline (close to the Gaussian prediction). (e) Conditional mean of the FDF of $q=(u_1''^2+u_2''^2)^{1/2}$ for $\Delta/\eta=63$ at the off-centerline position ($y/x=0.1$). The FDF without resolvable-scale rotation (star) is close to that in (b).

SGS energy k_L is $a^2\Delta^2/12$. If the x_1-x_2 coordinate system is isotropically oriented with respect to the ξ_1-ξ_2 coordinates, the VFJDF depends only on $|\mathbf{v}|$ and the normalized size of the uniform region is given as $|\mathbf{v}|/(2k_L)^{1/2}=|\mathbf{u}(\Delta/2)|/(2k_L)^{1/2}=(3/2)^{1/2}\approx 1.22$. For $|\mathbf{v}|/(2k_L)^{1/2}$ larger than this value, the FJDF decreases and vanishes beyond $|\mathbf{u}(\sqrt{2}\Delta/2)|/(2k_L)^{1/2}=3^{1/2}\approx 1.73$.

For the general case that the normal vector of the filter plane is randomly oriented with respect to the plane of strain, a and b are generally smaller and have different (random) values depending on the orientation. Consequently, the size of the uniform region of the FJDF will decrease and possibly vanish. This suggests that the random orientation of the flow structure might be a reason that the measured VFJDF has a somewhat smaller uniform region than predicted. In addition to the plane strain field there are fluctuations (of smaller amplitudes) in the SGS velocity which also tend to reduce the size of the uniform region. We note that a uniform

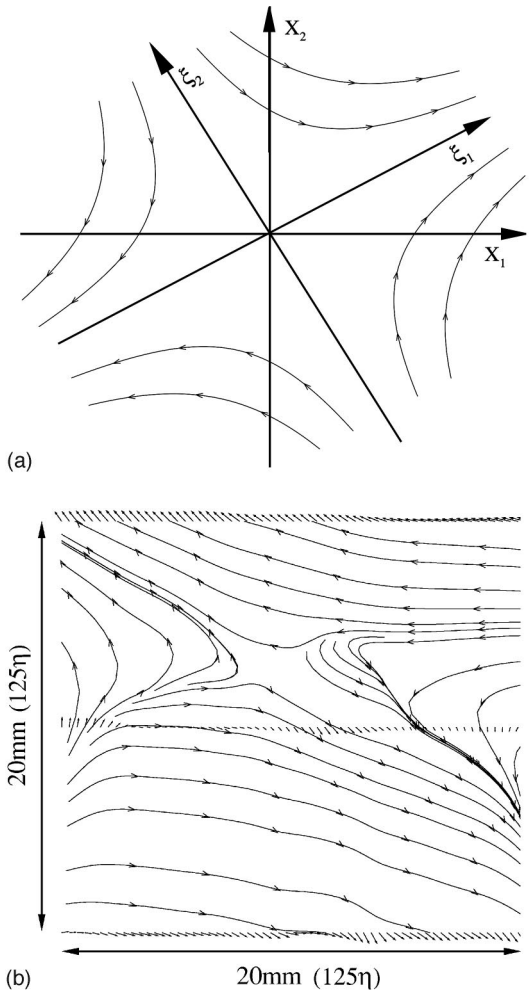

FIG. 5. (a) A plane strain field with a random orientation with respect to the laboratory coordinate system. (b) An example of conditional SGS velocity field with large $k_L(k_L/\langle k_L\rangle=4.6)$. The SGS velocity field is consistent with a plane strain field.

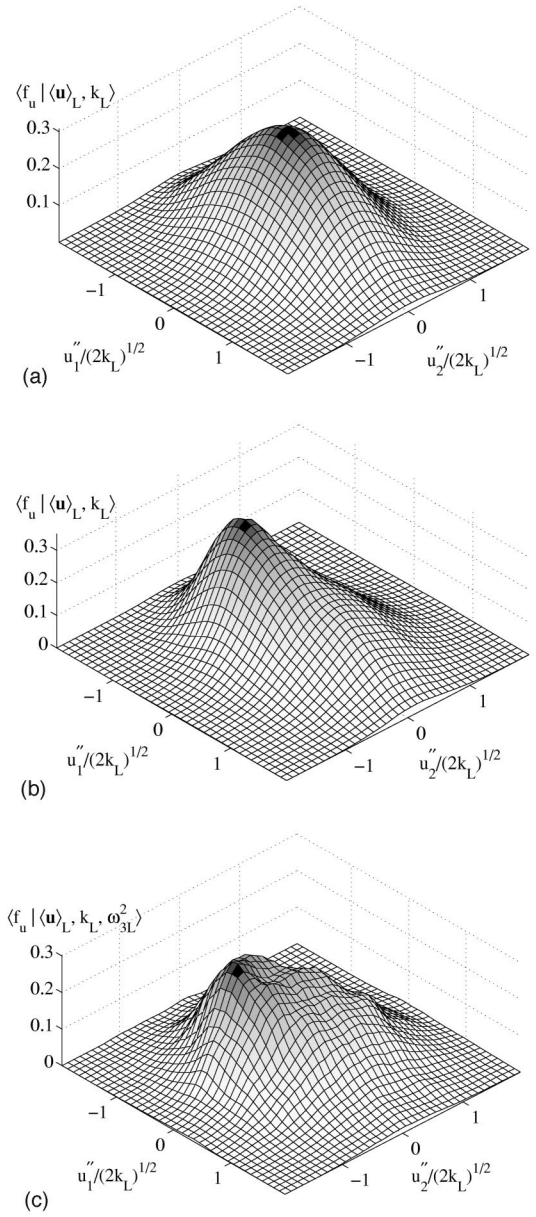

FIG. 6. Conditional mean of the VFJDF for $\Delta/\eta=63$ at the off-centerline position $(y/x=0.1)$ for $\langle u_1\rangle_L=\langle u_1\rangle$ and $\langle u_2\rangle_L=0$. (a) $k_L/\langle k_L\rangle=0.3$; (b) $k_L/\langle k_L\rangle=3.49$; (c) $k_L/\langle k_L\rangle=3.49$ and $\omega_3^2/\langle\omega_3^2|k_L\rangle<10^{-4}$. Also see Fig. 4(e).

VFJDF can also result from other flow structures with linear velocity variations such as solid-body rotation and axisymmetric contraction/expansion.

Converging-diverging flow structures (of integral-scale size) similar to a plane strain have been observed in regions between vortical structures in turbulent jets[39] and mixing layers.[40] The so-called ramp-cliff structures, which contain sharp scalar interfaces, are associated with converging-diverging structures.[39] In shear flows the structures are well organized and preferentially oriented. Thus, the variations of the orientation of the filter-plane normal vector relative to the structure are likely to be limited and so are the fluctuations in the parameters a and b. Therefore, an approximately uniform region of the VFJDF can be expected. In isotropic turbulence such a structure has also been shown to exist[41,42] and to cause ramp-cliffs when a mean scalar gradient is present.[43,44] However, the orientation of the structure is isotropically distributed. It would be interesting to see whether a uniform region of the VFJDF still exists. The VFJDF observed in the present study is consistent with the preferential orientations of organized structures. It also suggests that such a structure may also exist in the inertial range (but with larger strain rates) and might be the cause for the diffusion-layer-like structure previously observed.[35,43]

The VFJDF at the off-centerline location $(y/x=0.1)$ is also close to joint Gaussian for small k_L [Fig. 6(a)]. There is no correlation between the SGS velocity components. However, the FJDF does not have a uniform region when k_L is large [Fig. 6(b)]. Rather, it is somewhat similar to a ridge shape and there is a positive correlation coefficient of 0.072 between u_1'' and u_2''. The peak (near $u_1''=-0.5$ and $u_2''=-0.4$) is most likely due to the use of Taylor's hypothesis at off-centerline positions because negative u_1'' is associated with smaller convection velocity and smaller spatial extent, resulting in more concentrated velocity values. The lack of a uniform region in the VFJDF might be due to the rotation asso-

ciated with the mean shear at off-centerline locations. To examine this we compute the VFJDF with the square of the resolvable-scale vorticity component $\omega_{3L}^2=(\partial\langle u_1\rangle_L/\partial x_2-\partial\langle u_2\rangle_L/\partial x_1)^2$ as an additional conditioning variable. The VFJDF for $\omega_{3L}^2/\langle\omega_{3L}^2|k_L\rangle<10^{-4}$, i.e., for the SGS velocity without resolvable-scale rotation, begins to show a flat region [Fig. 6(c)], although the peak associated with Taylor's hypothesis is still present. The correlation coefficient between u_1'' and u_2'' is higher (0.14). The effects of removing rotation on the VFJDF are manifested more strongly in the FDF of q given in Fig. 4(e). The FDF conditioned on ω_{3L}^2 is not far from the centerline results in Fig. 4(b) for large k_L whereas the one without this condition is significantly different. Therefore, the rotation caused by the shear off the jet centerline appears to be the cause for the lack of a uniform region for the VFJDF in Fig. 6(b).

The approximately linear SGS velocity field implied by the uniform FJDF observed occurs when the SGS energy is large compared to its mean. Thus, the strain rate imposed by the structure ($|S|\sim k_L^{1/2}/\Delta$) is generally larger than the average turbulent strain rate associated with the filter scale ($\sim\langle k_L\rangle^{1/2}/\Delta$). Under such conditions the SGS turbulence is expected to be undergoing (local) rapid distortion (or extended rapid distortion). This situation is similar to that studied by Hunt and Carruthers[45] because the structure responsible for distorting the SGS turbulence is not the mean flow. For sufficiently large k_L values, the SGS turbulence is expected to evolve under rapid distortion. The local rapid distortion might also be related to the long-range triad interactions of velocity Fourier modes (modes with disparate wavenumbers) previously studied[46] since the approximately linear structure observed in the present study is likely to be much larger than the filter scale. The study in Ref. 46 showed that long-range interactions can play an important role in spectra energy transfer. When the strain rate of the large-scale structure is large, the long-range interactions are expected to dominate over the short-range triad (local) interactions, resulting in local rapid distortion.

The observed local rapid distortion has implications for SGS modeling. Equation (3) shows that the conditional pressure-strain-rate tensor is important for the evolution of the VFJDF. Under rapid distortion this tensor is dominated by the rapid pressure. Modeling the rapid pressure-strain-rate term is a major task in Reynolds stress closures. Since directional information is needed to describe turbulence under rapid distortion, one-point velocity PDF model is not sufficient. To overcome this difficulty, Van Slooten and Pope (1997) developed a velocity-wavevector PDF model which gives exact Reynolds stress evolution under the rapid distortion limit. The present study suggests that local rapid distortion (or its effects) exists even when the mean strain rate is not large. Therefore, it may be beneficial to adapt this model to LES so that the local rapid distortion effects can be taken into account. However, the cost of including the wavevector may be too high to be computationally attractive at present.

The local rapid distortion is also potentially important for modeling the SGS stress. Because under such conditions the evolution of the SGS turbulence is determined by the amount of strain applied, not the strain rate, the dynamics of the SGS stress for small and large SGS energy are expected to have very different characteristics. Thus eddy-viscosity-type models are generally inconsistent with rapid distortion.

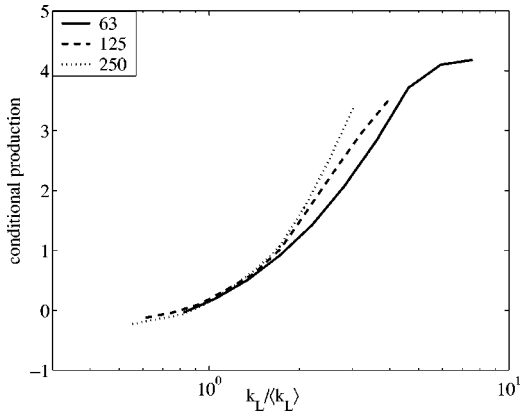

FIG. 7. Conditional production of SGS energy (energy transfer rate) normalized by the filtered energy dissipation rate, $\langle(\langle u_iu_j\rangle_L-\langle u_i\rangle_L\langle u_j\rangle_L)s_{ij}|k_L\rangle/\langle\epsilon_L|k_L\rangle$. The production exceeds the dissipation for large values of k_L, indicating nonequilibrium SGS velocity. The filter sizes are given in the legend.

B. The influence of the filtered energy dissipation rate

In turbulence under rapid distortion, the spectral energy transfer rate is small compared to the production due to the mean strain. Thus the turbulent fluctuations gain more energy than the spectral transfer (and than the dissipation) can remove, suggesting nonequilibrium turbulence. The SGS turbulence under rapid distortion is also found to be in nonequilibrium.[47] To determine whether the SGS turbulence under *local* rapid distortion is in nonequilibrium, we compare the production rate of the SGS energy, $\tau_{ij}s_{ij}$, to the filtered dissipation rate ϵ_L. Here τ_{ij} is defined as $\langle u_iu_j\rangle_L-\langle u_i\rangle_L\langle u_j\rangle_L$. We use $\frac{15}{6}(\tau_{11}s_{11}+2\tau_{12}s_{12}+\tau_{22}s_{22})$ and $5\nu[(\partial u_1/\partial x_1)^2+(\partial u_2/\partial x_1)^2]$ as surrogates for the full energy production and the full dissipation rate. Figure 7 gives the ratio of the conditional production of the SGS energy to the conditional dissipation conditional on the SGS energy. Indeed the conditional production exceeds the conditional dissipation when the SGS energy is larger than its mean value, indicating that the spectral transfer is not effective in responding to the increased SGS energy production and that the SGS turbulence is in nonequilibrium. This result is consistent with those for SGS turbulence under rapid distortion by the mean flow.[47] The nonequilibrium of the SGS velocity is similar to the nonequilibrium of the SGS scalar when the SGS variance is large.[18] Like the nonequilibrium SGS scalar which contains scalar structures (diffusion layers), the nonequilibrium SGS velocity also contains structures.

We note that although for the k_L values used in the present study (the maximum value that can ensure sufficient statistical convergence is limited by the size of our data set) the ratio of the conditional production to dissipation only goes up to $\approx$4.5, the results in Fig. 7 show that the ratio will continue to increase rapidly with k_L. Therefore, for suffi-

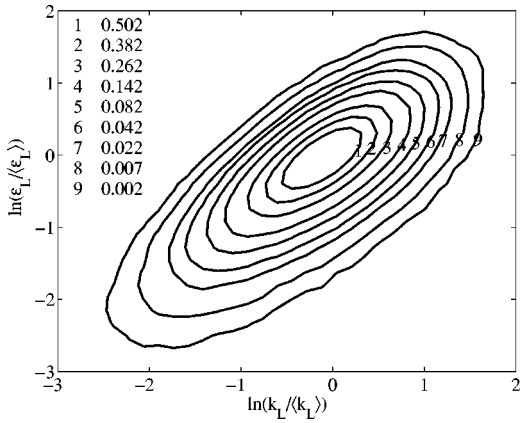

FIG. 8. JPDF of $\ln k_L$ and $\ln\epsilon_L$ for $\Delta/\eta=125$. The SGS turbulence is in nonequilibrium for large k_L/ϵ_L. The correlation coefficient for the variables is 0.720.

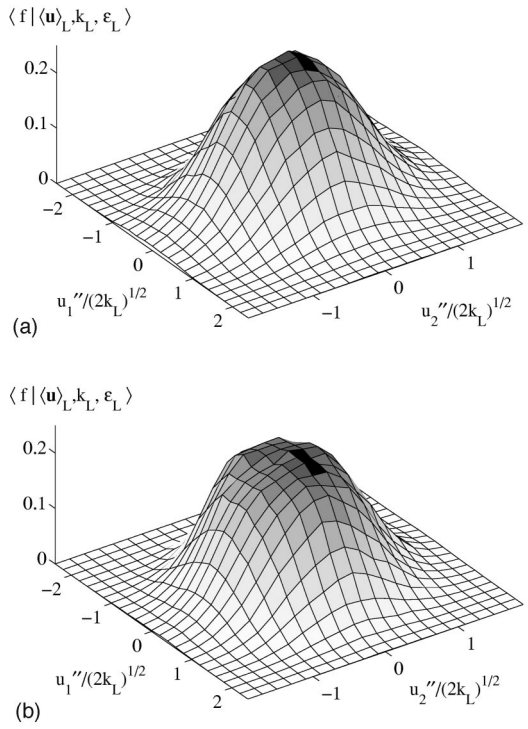

FIG. 9. VFJDF conditional on $\langle\mathbf{u}\rangle_L$, k_L, and ϵ_L for $\langle u_1\rangle_L=\langle u_1\rangle$, $\langle u_2\rangle_L=0$, and $k_L/\langle k_L\rangle=3.4$. The filter size is $\Delta/\eta=125$. (a) $\epsilon_L/\langle\epsilon_L\rangle=4.4$; (b) $\epsilon_L/\langle\epsilon_L\rangle=1.5$.

ciently large k_L (it appears that $k_L/\langle k_L\rangle>10$ is needed for the ratio to exceed a decade) the production will dominate over dissipation. Even at a value of $\approx 3-5$, only 20%–30% of the production (spectral transfer) reaches the dissipation scales. At the same time the FJDF is approaching the asymptotic top-hat shape, indicating that the production is beginning to dominate. Therefore, it is unlikely that the results will be qualitatively different for larger k_L values.

It is also worth noting that a large ratio of production to dissipation alone does not necessarily result in rapid distortion, as in the case of a homogeneous shear flow. This is probably related to the duration of the strain. Because the resolvable-scale strain rate is a fluctuating quantity and the duration of intense straining is generally short, it is unlikely that the SGS velocity will reach an asymptotic equilibrium state during the course of such straining. This is in contrast with a homogeneous shear flow, in which the strain rate is constant and the turbulent velocity reaches an asymptotic self-similar state. Therefore, despite the fact that production is larger than dissipation, rapid distortion might not properly describe the dynamic process in a homogeneous shear flow. Nonetheless, Maxey[48] obtained improved predictions of the results of Tavoularis and Corrsin[49] using rapid distortion theory (RDT) but with an effective strain, which is limited by the eddy turnover time, further demonstrating the role played by linear distortion.

To further examine effects of the nonequilibrium SGS turbulence on the VFJDF we compute the conditional VFJDF with the filtered dissipation ϵ_L used as an additional conditioning variable. The SGS dissipation time scale, k_L/ϵ_L, can be used as an indicator of the degree of the nonequilibrium: Large SGS time scale indicates that dissipation is not fast enough and thus the SGS turbulence is in nonequilibrium. It has been observed experimentally that the conditional PDFs of velocity increments have strong dependence on both k_L and ϵ_L.[26] The filtered energy dissipation is also important from a modeling point of view as it is a key parameter in LES employing the Langevin model.[13,50] It is also an important variable for the inertial-range dynamics (in the context of Kolmogorov's refined similarity hypotheses[51]). Figure 8 shows that the JPDF of $\ln k_L$ and $\ln\epsilon_L$ is approximately joint normal. There is a strong correlation between $\ln k_L$ and $\ln\epsilon_L$ because k_L can be related to ϵ_L by Kolmogorov's refined similarity hypotheses. The correlation coefficients for $\Delta/\eta=63$, 125, and 250 are 0.78, 0.72 and 0.644, respectively. The lower correlation values for the larger filter sizes are probably because they are too close to the integral length scale and the fluctuations in both k_L and ϵ_L are smaller. The SGS turbulence is expected to be in equilibrium toward upper left corner (small k_L/ϵ_L values) and in nonequilibrium and under local rapid distortion toward lower right corner (large k_L/ϵ_L values).

In Fig. 9 the conditional VFJDF for $k_L/\langle k_L\rangle=3.38$ and two $\epsilon_L/\langle\epsilon_L\rangle$ values are given. For $\epsilon_L/\langle\epsilon_L\rangle=4.40$ the VFJDF is somewhat close to a joint-Gaussian shape. However, as ϵ_L decreases ($\epsilon_L/\langle\epsilon_L\rangle=1.45$) an approximately uniform region begins to emerge in the VFJDF; thus the VFJDF is similar to that conditioned on large k_L alone. Because the SGS velocity field changes toward nonequilibrium as ϵ_L decreases, the results further show that the VFJDF is uniform when the SGS velocity is in strong nonequilibrium.

To quantify the dependence of the shape of the VFJDF on k_L and ϵ_L, we use two slices of the VFJDF going through the origin in the v_1 and v_2 directions, respectively. We compute the conditional kurtosis and skewness of the VFJDF, $K_{u_1|u_2}$ and $S_{u_1|u_2}$ (for $u_2=0$), which can be obtained from the conditional fourth and third moments of $\langle f_{u_1|u_2}(v_1)|k_L,\epsilon_L,\langle\mathbf{u}\rangle_L\rangle$, normalized by the second moment raised to the proper power, where $f_{u_1|u_2}$ is the FDF of the u_1 component conditional on the u_2 component (essentially a slice in the u_1 direction). The conditional kurtosis and skewness $K_{u_2|u_1}$ and $S_{u_2|u_1}$ can also be obtained in the same way.

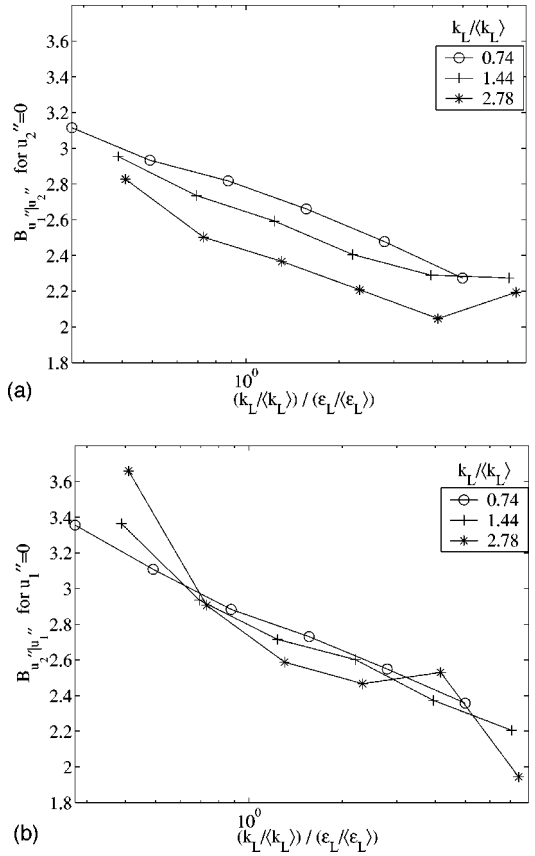

FIG. 10. The parameters B as a function of k_L/ϵ_L for $\Delta/\eta=125$ for different k_L values. The collapse of the curves indicates that the VFJDF can largely be characterized by $k_L/\epsilon_L/(\langle k_L\rangle/\langle\epsilon_L\rangle)$.

We combine K and S to form a parameter $B=K-S^2$, proposed by Atkinson.[52] This parameter takes the value of unity for a double-delta PDF regardless of its symmetry, thus is a better measure of the intermittency (or lack of) than the kurtosis. For a uniform distribution B has a value of 1.8. It has been used to characterize the bimodal scalar FDF (Ref. 17) and velocity increment PDF.[26]

We now examine $B_{u_1|u_2}$ for $u_2''=0$ and $B_{u_2|u_1}$ for $u_1''=0$. If the VFJDF is perfectly uniform both parameters have the value of 1.8. It is observed that B generally decreases with ϵ_L, consistent with the observation that the VFJDF changes towards a uniform shape as ϵ_L decreases. Due to the opposite trends of B with respect to k_L and ϵ_L, we plot $B_{u_1|u_2}$ and $B_{u_2|u_1}$ against k_L/ϵ_L for three k_L values. Figure 10 shows that both $B_{u_1|u_2}$ and $B_{u_2|u_1}$ decrease as k_L/ϵ_L increases. Furthermore, the curves for $B_{u_2|u_1}$ appear to collapse for different k_L values, although the results for $B_{u_1|u_2}$ still show some k_L dependence. Nonetheless, these results indicate that k_L/ϵ_L alone can largely characterize the shape of the VFJDF. Specifically, the VFJDF is uniform as long as k_L/ϵ_L is large, i.e., when the SGS velocity is in strong nonequilibrium, regardless of the value of k_L. This condition is less restrictive than that of $k_L/\langle k_L\rangle \gg 1$. The observed importance of k_L/ϵ_L in determining $B_{u_1|u_2}$ and $B_{u_2|u_1}$ suggests that the degree of nonequilibrium is important for determining the distribution of the SGS velocity field.

The dependence of the SGS velocity on k_L and ϵ_L is consistent with that of conditional velocity increment. It has been previously observed experimentally that the conditional PDF of velocity increments has a strong dependence on both k_L and ϵ_L:[26] as the filtered energy dissipation decreases or increases, the conditional increment PDF generally changes towards bimodal or Gaussian shapes, respectively. In previous studies of scalar FDF and its transport equation,[17,18] the filtered scalar dissipation rate was found to have a strong influence when used as a conditioning variable in addition to the SGS scalar variance and the resolvable-scale scalar. These results provide further evidence that the nonequilibrium plays a key role in determining the local turbulence fields.

C. The conditionally filtered viscous acceleration and dissipation

In the present study two (partial) components of the viscous acceleration are measured. The conditionally filtered viscous acceleration, $\langle \nu(\partial^2 u_1/\partial x_1^2, \frac{1}{2}\partial^2 u_2/\partial x_1^2)\,|\,u_1,u_2\rangle_L$, conditional on the velocity components, represents the transport velocity of the VFJDF by viscous acceleration in the velocity space and is shown in Fig. 11 as streamline plots. A factor of $1/2$ is used for the u_2 component because for isotropic turbulence its rms is twice that of the u_1 component. The magnitude of the vector field, normalized by $(2k_L)^{1/2}/\langle\epsilon_L|k_L\rangle$, is given as gray scale isocontours. The streamlines generally flow towards a stagnation point, which is approximately at the center of the VFJDF. The magnitude of the acceleration increases with the magnitude of the velocity. This dependence is similar to that of the scalar diffusion on the value of the scalar.[53–55] The conditional viscous acceleration in the velocity JPDF equation, $\langle \nu(\partial^2 u_1/\partial x_1^2, \frac{1}{2}\partial^2 u_2/\partial x_1^2)\,|\,u_1,u_2\rangle$, also has similar properties [Fig. 11(c)]. The normalized magnitude of the conditionally filtered viscous acceleration increases faster for larger SGS energy. This is probably because the local rapid distortion at large SGS energy causes the SGS fluctuations and accelerations to increase, although the linear portion of the SGS velocity does not directly contribute to viscous acceleration. The observed rate of increase might also be partially due to the decrease in the normalized sample-space variable $\mathbf{v}/(2k_L)^{1/2}$. We note that although the conditional viscous acceleration is non-negligible, the rms viscous acceleration becomes smaller than the rms pressure gradient as Reynolds number increases.[56]

The conditionally filtered dissipation tensor $\langle\epsilon_{ij}|u_1,u_2\rangle_L$ provides an alternative to the conditionally filtered viscous acceleration to close the VFJDF equation. Figure 12 shows the surface plots for the conditionally filtered energy dissipation rate $\langle\epsilon|u_1,u_2\rangle_L$ normalized by $\langle\epsilon_L|k_L\rangle$. In general the dissipation increases with u_1. For small SGS energy the surface is concave, similar to the dependence of the scalar dissipation on the scalar values for small SGS variance. The surface plot for the conditional energy dissipation $\langle\epsilon|u_1,u_2\rangle$, which appears in the velocity JPDF equation, also has a similar shape. For large SGS energy there is a slight bulge in the center portion of the surface. This suggests that the local

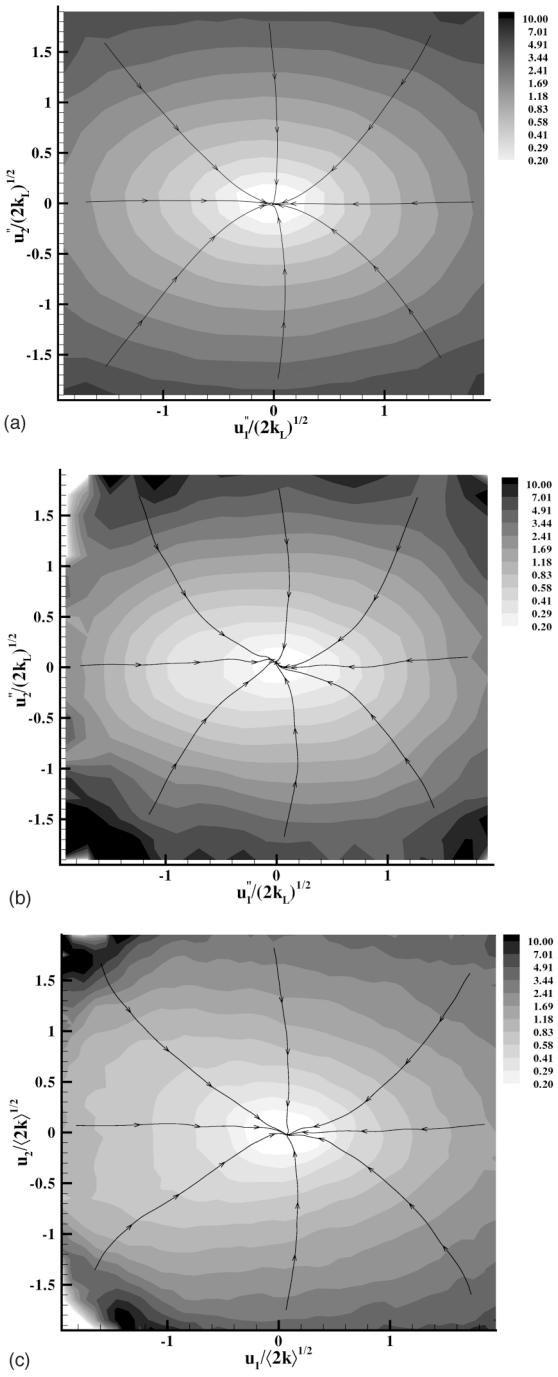

FIG. 11. Streamline plots of the conditional filtered viscous acceleration for $\Delta/\eta=125$, $\langle\langle \nu(\partial^2 u_1/\partial x_1^2, \frac{1}{2}\partial^2 u_2/\partial x_1^2)|u_1,u_2\rangle_L|\langle\mathbf{u}\rangle_L, k_L\rangle(2k_L)^{1/2}/\langle\epsilon_L|k_L\rangle$. $\langle u_1\rangle_L = \langle u_1\rangle$ and $\langle u_2\rangle_L = 0$ (a and b). (a) $k_L/\langle k_L\rangle = 1.2$, (b) $k_L/\langle k_L\rangle = 4.6$. (c) The conditional viscous acceleration $\langle \nu(\partial^2 u_1/\partial x_1^2, \frac{1}{2}\partial^2 u_2/\partial x_1^2)|u_1,u_2\rangle \times(2\langle k\rangle)^{1/2}/\langle\epsilon\rangle$. The magnitudes of these variables are given as gray scales.

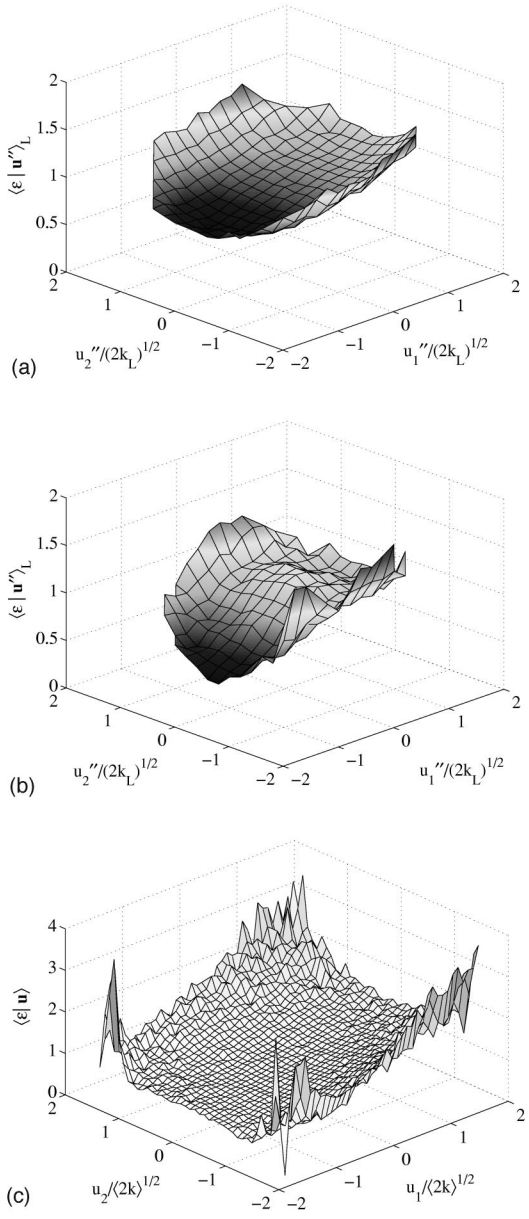

FIG. 12. The conditionally filtered energy dissipation rate $\langle\langle\epsilon|u_1,u_2\rangle_L|\langle\mathbf{u}\rangle_L,k_L\rangle/\langle\epsilon_L|k_L\rangle$ (a and b). (c) The conditional energy dissipation rate $\langle\epsilon|u_1,u_2\rangle/\langle\epsilon\rangle$. The conditions are the same as in Fig. 11.

velocity field responsible for the large strain rate deviates somewhat from a linear field because the dissipation is constant in such a field. Nonetheless, the deviation is small as indicated by uniform portion of the conditional VFJDF. The moderate dependence of dissipation on the SGS velocity suggests that the current practice of modeling the dissipation independent of the velocity is largely justified.

The isotropic form of the second-order conditionally filtered energy dissipation tensor $\langle\boldsymbol{\epsilon}_{ij}|\mathbf{u}=\mathbf{v}\rangle_L$ can be written as

$$\langle\boldsymbol{\epsilon}_{ij}|\mathbf{u}=\mathbf{v}\rangle_L = [\langle\boldsymbol{\epsilon}_{LL}|v\rangle_L - \langle\boldsymbol{\epsilon}_{NN}|v\rangle_L]\frac{v_i v_j}{v^2} - \langle\boldsymbol{\epsilon}_{NN}|v\rangle_L\delta_{ij}, \quad (5)$$

where $\boldsymbol{\epsilon}_{LL}$ and $\boldsymbol{\epsilon}_{NN}$ are the energy dissipation components that involve the velocity components along (longitudinal) and normal (transverse) to the direction of $\mathbf{v}$, respectively. We note that local isotropy requires that the unconditioned mean $\langle\boldsymbol{\epsilon}_{ij}\rangle$ vanishes for $i\neq j$. However, if the dissipation tensor $\boldsymbol{\epsilon}_{ij}$ is statistically dependent on $\mathbf{u}$, $\langle\boldsymbol{\epsilon}_{ij}|\mathbf{u}=\mathbf{v}\rangle_L$ can still have nonzero values consistent with the isotropic form. In the present study two velocity components and their streamwise derivatives are available. The off-diagonal component $\langle\boldsymbol{\epsilon}_{12}|u_1,u_2\rangle_L$ is computed using $\boldsymbol{\epsilon}_{12}=\nu(\partial u_1/\partial x_1)(\partial u_2/\partial x_1)$

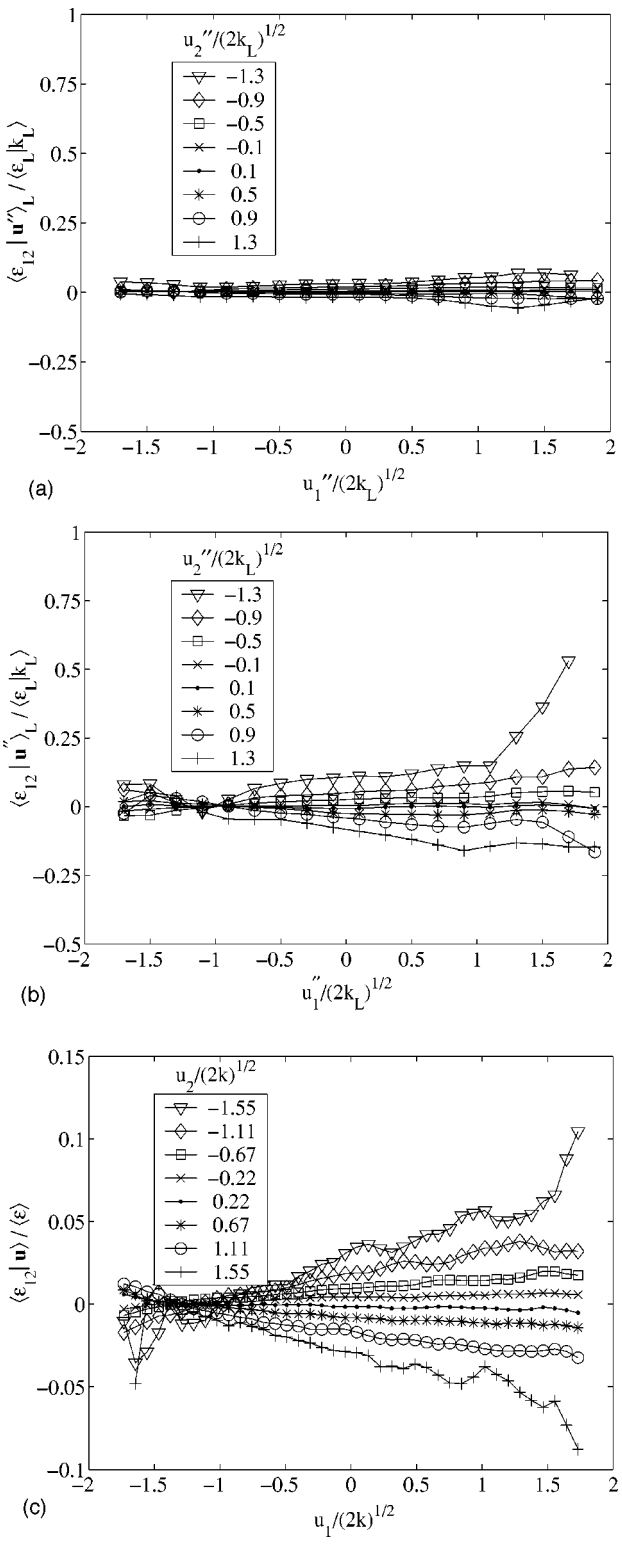

FIG. 13. The off-diagonal component of the conditionally filtered dissipation rate tensor $\langle\langle\epsilon_{12}|u_1,u_2\rangle|\langle\mathbf{u}\rangle_L,k_L\rangle/\langle\epsilon_L|k_L\rangle$ (a and b). (c) The off-diagonal component of the conditional dissipation rate tensor $\langle\epsilon_{12}|u_1,u_2\rangle/\langle\epsilon\rangle$. The $u_2''/(2k_L)^{1/2}$ values are given in the legend. The conditions are the same as in Fig. 11.

since the cross-stream derivatives are not available in this study. Figure 13(a) shows that for small k_L the magnitude of $\langle\epsilon_{12}|u_1,u_2\rangle_L$ is generally less than 0.1, similar to the conditional cross-dissipation $\langle\epsilon_{12}|u_1,u_2\rangle$ shown in Fig. 13(c). For $k_L/\langle k_L\rangle=4.6$, $\langle\epsilon_{12}|u_1,u_2\rangle_L$ appears to be odd in both u_1'' and u_2'': it tends to have negative values when u_1'' is negative and u_2'' is positive, and vice versa, qualitatively consistent with the isotropic form in Eq. (5). However, its magnitude reaches ≈ 0.2, larger than the results for small k_L. Considering that only one component of ϵ_{12} is used here, the magnitude is not small compared to the diagonal components. Therefore, it is potentially important to consider the off-diagonal components in modeling the dissipation tensor, at least for the Reynolds number studied.

IV. CONCLUSIONS

In this work the velocity filtered joint density function and its transport equation as well as the structure of the SGS velocity field are studied. Data obtained in the fully developed region of a turbulent air jet ($\mathrm{Re}_j=40\,000$) are used in the analyses. An array consisting of three X-wires aligned in the cross-stream direction is employed in conjunction with Taylor's hypothesis to form a two-dimensional filter to obtain the VFJDF and other filtered variables. The width of the filter is varied from 63 to 250 Kolmogorov scales by changing the spacing between the X wires.

The VFJDF and its transport equation are studied by analyzing their conditional means with the resolvable-scale velocity ($\langle u_i\rangle_L$), the SGS turbulent kinetic energy (k_L), and the filtered energy dissipation rate (ϵ_L) as conditioning variables. The results show that these conditional statistics reveal new structures of the SGS velocity and characteristics of the VFJDF which are important for SGS modeling. Specifically, the conditional VFJDF is found to be close to joint normal when k_L is small, similar to the velocity JPDF generally observed in fully developed turbulent flows. For large k_L the VFJDF obtained on the jet centerline has a uniform region. Such a distribution has not been observed in fully developed flows and suggests that the SGS velocity under such conditions contains distinct structures. One possibility is an approximately linear structure such as plane strain and solid body rotation. These structures could result from known coherent structures in turbulent jets and regions between them. The VFJDF obtained at the off-centerline location ($y/x=0.1$) does not have a uniform region, probably due to the resolvable-scale rotation associated with mean shear. When the SGS velocity fields without resolvable-scale rotation are used to obtain the VFJDF, a uniform region begins to emerge at large SGS energy, indicating that the SGS turbulence is still under rapid distortion.

Since the uniform VFJDF and the linear structures occur at large k_L values, we argue that the SGS turbulence is undergoing local rapid distortion similar to that described by Hunt and Carruthers.[45] The SGS velocity gains significant amount of energy from the structures and the gain exceeds the dissipation, resulting in nonequilibrium. Thus the degree of nonequilibrium may be used as an indicator of the local rapid distortion. Further analyses of the VFJDF using ϵ_L as an additional conditioning variable show that the degree of nonequilibrium largely determines the shape of the VFJDF and therefore the structure of the SGS velocity fields.

The conditional dissipation tensor in the VFJDF equation shows some dependence on the SGS velocity, especially for large SGS energy. In particular, the off-diagonal component (ϵ_{12}) is significant compared to the diagonal components (the energy dissipation), suggesting that it may have non-negligible influence on the VFJDF, at least for the Reynolds number studied.

The local rapid distortion occurring at large k_L has strong implications for SGS modeling. Evolution of turbulence under rapid distortion is determined by the amount and geometry of the strain, independent of the strain rate. The VFJDF equation contains no directional information, therefore is insufficient to describe turbulence under rapid distortion. The velocity-wavevector PDF model developed by Van Slooten and Pope gives exact evolution of Reynolds stress, therefore it may be beneficial if adapted to model the VFJDF. However, the added computational costs may limit its practical applicability. In addition, eddy-viscosity models (often used in LES of nonreacting flows) relate the SGS stress to the resolvable-scale strain rate, therefore are qualitatively incorrect under the rapid distortion limit. To overcome this limitation, additional variables containing directional information can be used to supplement such models.[57]

The present study also has implications for studying and modeling the velocity-scalar FJDF for turbulent reacting flows. Since the diffusion layers (ramp-cliffs) in scalar fields may be related to converging-diverging structures, the approximately linear SGS velocity at large SGS energy can potentially have a strong influence on the SGS scalar.

ACKNOWLEDGMENTS

The support of the Air Force Office of Scientific Research under Grant No. F-49620-02-1-0130 to Clemson University and Grant No. F-49620-00-1-0171 to Cornell University (Dr. Julian M. Tishkoff, program manager) is gratefully acknowledged.

[1] P. Givi, "Model free simulations of turbulent reacting flows," Prog. Energy Combust. Sci. **15**, 1 (1989).
[2] S. B. Pope, in *Proceedings of the 23rd Symposium (International) on Combustion* (1990), pp. 591–612.
[3] F. Gao and E. E. O'Brien, "A Large-eddy simulation scheme for turbulent reacting flows," Phys. Fluids A **5**, 1282 (1993).
[4] C. Madnia and P. Givi, in *Large Eddy Simulation of Complex Engineering and Geophysical Flows*, edited by B. Galperin and S. Orszag (Cambridge University Press, Cambridge, 1993), pp. 315–346.
[5] S. Menon, P. A. McMurtry, and A. K. Kerstein, in *Large Eddy Simulation of Complex Engineering and Geophysical Flows*, edited by B. Galperin and S. A. Orszag (Cambridge University Press, Cambridge, 1993), pp. 287–314.
[6] A. W. Cook and J. J. Riley, "A subgrid model for equilibrium chemistry in turbulent flows," Phys. Fluids **6**, 2868 (1994).
[7] S. I. Moller, E. Lundgren, and C. Fureby, in *Proceedings of the Twenty-Sixth Symposium (International) on Combustion* (1993), pp. 241–248.
[8] J. Jiménez, A. Liñán, M. M. Rogers, and F. J. Higuera, "A priori testing of subgrid models for chemically reacting non-premixed turbulent shear flows," J. Fluid Mech. **349**, 149 (1997).
[9] A. W. Cook and J. J. Riley, "Subgrid-scale modeling for turbulent reacting flows," Combust. Flame **112**, 593 (1998).
[10] P. J. Colucci, F. A. Jaberi, P. Givi, and S. B. Pope, "Filtered density function for large eddy simulation of turbulent reacting flows," Phys. Fluids **10**, 499 (1998).
[11] P. E. DesJardin and S. H. Frankel, "Large eddy simulation of a nonpremixed reacting jet: Application and assessment of subgrid-scale combustion models," Phys. Fluids **10**, 2298 (1998).
[12] W. K. Bushe and H. Steiner, "Conditional moment closure for large eddy simulation of nonpremixed turbulent reacting flows," Phys. Fluids **11**, 1896 (1999).
[13] L. Y. M. Gicquel, P. Givi, F. A. Jaberi, and S. B. Pope, "Velocity filtered density function for large eddy simulation of turbulent flows," Phys. Fluids **14**, 1196 (2002).
[14] H. Pitsch, in *Proceedings of the Twenty-Ninth Symposium (International) on Combustion* (2002), pp. 1971–1978.
[15] M. R. H. Sheikhi, T. G. Drozda, P. Givi, and S. B. Pope, "Velocity-scalar filtered density function for large eddy simulation of turbulent flows," Phys. Fluids **15**, 2321 (2003).
[16] S. B. Pope, "PDF methods for turbulent reacting flows," Prog. Energy Combust. Sci. **11**, 119 (1985).
[17] C. Tong, "Measurements of conserved scalar filtered density function in a turbulent jet," Phys. Fluids **13**, 2923 (2001).
[18] D. Wang and C. Tong, "Conditionally filtered scalar dissipation, scalar diffusion, and velocity in a turbulent jet," Phys. Fluids **14**, 2170 (2002).
[19] C. Tong, "Galilean invariance of velocity probability density function transport equation," Phys. Fluids **15**, 2073 (2003).
[20] D. C. Haworth and S. B. Pope, "A generalized Langevin model for turbulent flows," Phys. Fluids **29**, 387 (1986).
[21] S. Tavoularis and S. Corrsin, "Experiments in nearly homogeneous turbulent shear flow with a uniform mean temperature gradient. Part 2. The fine structure," J. Fluid Mech. **104**, 349 (1981).
[22] K. S. Venkataramani, N. K. Tutu, and R. Chevray, "Probability distributions in a round turbulent jet," Phys. Fluids **18**, 1413 (1975).
[23] P. K. Yeung, "Lagrangian investigations of turbulence," Annu. Rev. Fluid Mech. **34**, 115 (2002).
[24] V. Eswaran and S. B. Pope, "Direct numerical simulations of the turbulent mixing of a passive scalar," Phys. Fluids **31**, 506 (1988).
[25] C. Meneveau and J. O'Neil, "Scaling laws of the dissipation rate of the turbulent subgrid-scale kinetic energy," Phys. Rev. E **49**, 2866 (1994).
[26] H. Zhang and C. Tong, "On conditional velocity increment statistics," Phys. Fluids **15**, 1676 (2003).
[27] I. Wygnanski and H. Fiedler, "Some measurements in the self-preserving jet," J. Fluid Mech. **38**, 577 (1969).
[28] N. R. Panchapakesan and J. L. Lumley, "Turbulence measurements in axisymmetric jet of air and helium. Part 1. air jet," J. Fluid Mech. **246**, 197 (1993).
[29] H. J. Hussein, S. P. Capp, and W. K. George, "Velocity measurements in a high-Reynolds-number, momentum-conserving, axisymmetric, turbulent jet," J. Fluid Mech. **258**, 31 (1994).
[30] C. Tong, J. C. Wyngaard, S. Khanna, and J. G. Brasseur, "Resolvable- and subgrid-scale measurement in the atmospheric surface layer: Technique and issues," J. Atmos. Sci. **55**, 3114 (1998).
[31] C. Tong, J. C. Wyngaard, and J. G. Brasseur, "Experimental study of subgrid-scale stress in the atmospheric surface layer," J. Atmos. Sci. **56**, 2277 (1999).
[32] F. Porté-Agel, M. B. Parlange, C. Meneveau, W. E. Eichinger, and M. Pahlow, "Subgrid-scale dissipation in the atmospheric surface layer: Effects of stability and filter dimension," J. Atmos. Sci. **57**, 75 (2000).
[33] S. Cerutti and C. Meneveau, "Statistics of filtered velocity in grid and wake turbulence," Phys. Fluids **12**, 1143 (2000).
[34] S. Cerutti, C. Meneveau, and O. M. Knio, "Spectral and hyper eddy viscosity in high-Reynolds-number turbulence," J. Fluid Mech. **421**, 307 (2000).
[35] A. G. Rajagopalan and C. Tong, "Experimental investigation of scalar-scalar-dissipation filtered joint density function and its transport equation," Phys. Fluids **15**, 227 (2003).
[36] H. Tennekes and J. L. Lumley, *A First Course in Turbulence* (MIT Press, Cambridge, MA, 1972).
[37] L. W. B. Browne, R. A. Antonia, and L. P. Chua, "Calibration of X-probes for turbulent flow measurements," Exp. Fluids **7**, 201 (1989).
[38] C. Meneveau, "Statistics of turbulence subgrid-scale stress: Necessary conditions and experimental tests," Phys. Fluids **6**, 815 (1994).
[39] R. A. Antonia, A. J. Chambers, D. Britz, and L. W. B. Browne, "Organized structures in a turbulent plane jet: topology and contributions to momentum and heat transport," J. Fluid Mech. **172**, 211 (1986).

[40]G. L. Brown and A. Roshko, "On density effects and large scale structure in turbulent mixing layers," J. Fluid Mech. **64**, 775 (1974).
[41]G. R. Ruetsch and M. R. Maxey, "Small-scale features of vorticity and passive scalar fields in homogeneous isotropic turbulence," Phys. Fluids A **3**, 1587 (1991).
[42]G. R. Ruetsch and M. R. Maxey, "The evolution of small-scale structures in homogeneous isotropic turbulence," Phys. Fluids A **4**, 2747 (1992).
[43]C. Tong and Z. Warhaft, "On passive scalar derivative statistics in grid turbulence," Phys. Fluids **6**, 2165 (1994).
[44]Z. Warhaft, "Passive scalars in turbulent flows," Annu. Rev. Fluid Mech. **32**, 203 (2000).
[45]J. C. R. Hunt and D. J. Carruthers, "Rapid distortion theory and the problem of turbulence," J. Fluid Mech. **212**, 497 (1990).
[46]P. K. Yeung and J. G. Brasseur, "The response of isotropic turbulence to isotropic and anisotropic forcing at the large scales," Phys. Fluids A **3**, 884 (1991).
[47]S. Liu, J. Katz, and C. Meneveau, "Evolution and modeling of subgrid scales during rapid distortion of turbulence," J. Fluid Mech. **387**, 281 (1999).
[48]M. R. Maxey, "Distortion of turbulence in flows with parallel streamlines," J. Fluid Mech. **124**, 261 (1982).
[49]S. Tavoularis and S. Corrsin, "Experiments in nearly homogeneous turbulent shear flow with a uniform temperature gradient. Part 1," J. Fluid Mech. **104**, 311 (1981).
[50]S. B. Pope, "Lagrangian PDF methods for turbulent flows," Annu. Rev. Fluid Mech. **26**, 23 (1994).
[51]A. N. Kolmogorov, "A refinement of previous hypothesis concerning the local structure of turbulence in a viscous incompressible fluid at high Reynolds number," Phys. Fluids **13**, 82 (1962).
[52]A. R. Masri, R. W. Dibble, and R. S. Barlow, "The structure of turbulent nonpremixed flames revealed by Raman–Rayleigh–LIF measurements," Prog. Energy Combust. Sci. **22**, 307 (1996).
[53]R. S. Miller, S. H. Frankel, C. K. Madnia, and P. Givi, "Johnson–Edgeworth translation for probability modeling of binary mixing in turbulent flows," Combust. Sci. Technol. **91**, 21 (1993).
[54]C. Tong and Z. Warhaft, "Scalar dispersion and mixing in a jet," J. Fluid Mech. **292**, 1 (1995).
[55]M. R. Overholt and S. B. Pope, "Direct numerical simulation of a passive scalar with imposed mean gradient in isotropic turbulence," Phys. Fluids **8**, 3128 (1996).
[56]P. Vedula and P. K. Yeung, "Similarity scaling of acceleration and pressure statistics in numerical simulations of isotropic turbulence," Phys. Fluids **11**, 1208 (1999).
[57]W. C. Reynolds, C. A. Langer, and S. C. Kassinos, "Structure and scale in turbulence modeling," Phys. Fluids **14**, 2485 (2002).